Ab initio embedded cluster study of optical second-harmonic generation below the gap of a NiO(001) surface

K. Satitkovitchai, Y. Pavlyukh, and W. Hübner
Max-Planck-Institut für Mikrostrukturphysik, Weinberg 2, D-06120 Halle, Germany
(Received 25 June 2002; revised manuscript received 14 October 2002; published 22 April 2003)

An embedded cluster approach was applied to study the electronic excitations on the NiO(001) surface. Using a quantum chemical calculation, a small $(NiO_5)^{8-}$ cluster was embedded in a set of point charges to model the NiO(001) surface. Starting from the unrestricted Hartree-Fock level of theory, we calculate the ground-state properties to provide some insight into electronic structure and excitation. We estimate the excitation energies and oscillator strengths using the single excitation configuration-interaction (CIS) technique. Our results show that the CIS method is reasonably accurate for estimating the low-lying *d-d* excitations below the gap. We then demonstrate the electron correlation effects on the *d-d* transitions at several levels of *ab initio* correlated theory [CID (with all double substitutions), CISD (with all single and double substitutions), (quadratic) QCISD, and (with all single, double, and triple substitutions) QCISD (*T*)]. The electron correlation tends to decrease the magnitude of *d*-electron excitation energies. Using the many-body wave functions and energies resulting from CID and QCISD(*T*) calculations, we compute the second harmonic generation (SHG) tensor for the NiO(001) surface. In contrast to bulk NiO, where the SHG response is forbidden within the electric-dipole approximation because of the inversion symmetry, the C_{4v} symmetry of the surface leads to five nonzero tensor elements. From that, the intensity of the nonlinear optical response as a function of photon energy at different polarizations of the incident and outgoing photons is obtained. This quantity can be directly measured in experiment, and we suggest possible conditions in order to detect it.

DOI: 10.1103/PhysRevB.67.165413 PACS number(s): 72.80.Ga, 71.15.Qe, 42.65.An, 31.15.Ar

I. INTRODUCTION

Future computer memories require a merger between the existing technologies of permanent (magnetic) information storage and random access memories. The envisaged magnetic random access memories.[1] are assumed to be faster and nonvolatile while beating the contemporary designs also in storage density. One of the most successful approaches so far is based on tunneling magnetoresistance junctions, where the relative magnetization direction of two ferromagnetic metallic layers governs the tunneling rate through an insulator placed between them (reading). The magnetization of one of the ferromagnetic layers can be adjusted (writing), while the other ferromagnetic layer is pinned usually by an antiferromagnet. For such a design, transition-metal oxides (TMO's) such as NiO are of interest since they are *both* insulating and antiferromagnetic. One of the crucial elements of the proposed device is the metal-TMO interface. The properties of this interface can conveniently be assessed by the technique of optical SHG, which is interface sensitive and can easily access antiferromagnetism.[2–4] These technological developments require a detailed theoretical understanding of the nonlinear optical processes on TMO surfaces. This is, however, a formidable task for two main reasons: (i) an electronic *ab initio* theory of the nonlinear magneto-optical response at solid surfaces has long been in its infancy and is just about to emerge due to the enormously high-precision requirements for obtaining reliable results and (ii) transition-metal oxides are notorious examples of strongly correlated electron systems that have escaped a description by even phenomenological many-body theories since the 1960s.[5–7]

In view of these difficulties, any tractable theoretical attempt at the theoretically, experimentally, and technologically interesting problem of a first-principles description of nonlinear magneto-optics from the surface of NiO(001) has to start at the entry level and to leave aside a great deal of the sophistication underlying both subproblems individually, viz (i) the consistent many-body description of the electronic properties of transition-metal oxide surfaces and (ii) the *ab initio* theory of nonlinear optics from a magnetic solid.

In this study, we make the first step towards an *ab initio* theory of SHG from TMO surfaces and calculate optically active states on the NiO(001) surface. We first perform the computation of optical properties such as discrete excitations below the gap and continuous excitation spectra above the gap for NiO(001) within the configuration-interaction singles (CIS) framework.[8] In this method, the CIS wave function is expressed as a combination of all determinants obtained by replacing one occupied orbital [from the ground-state Hartree-Fock (HF) determinant] with a virtual orbital. The single excitations do not only cause a shift of excitation energy but also allow a proper calculation of optical spectra in the UV and the visible range. In our calculation, we do not only obtain an *ab initio* calculation to estimate *d-d* transitions, but we assess the relative importance of the different electronic correlation. In order to do so, *d-d* excitation energies are also determined on several correlated levels of theory such as CI (configuration interaction) and QCI (quadratic configuration interaction) approaches.[9,10]

Our main method, the (with all single, double, and triple substitutions) QCISD (*T*) approach, accounts for correlations almost fully and possesses a large number of advantages compared to lower-order CI calculations such as CIS, CID (with all double substitutions), and CISD (with all single and double substitutions). For example, it is size consistent. This

method was established by Pople *et al.*[10] in 1987 and since then, it has successfully been applied to a variety of systems. In the case of simple molecules, a comparison with a full CI calculation is possible and shows good agreement. The results for larger systems including metal oxide clusters are presented in the literature as well (such as Ref. 11). The scaling of the QCISD method with N^6 (where N is the number of basis functions in the system) is comparable with the coupled cluster (CC) approach of the same level (i.e., CCSD).[12]

Then, we turn to step (ii) for developing an *ab initio* theory of SHG in NiO. We calculate the nonlinear optical response following an expression developed by Hübner and Bennemann.[13]

II. COMPUTATIONAL METHOD

A. Theoretical framework

This section contains a brief outline of two of the theoretical methods that are performed in this work.

1. Ab initio correlated electron theory

In *ab initio* quantum chemistry, the exact level energy $E(\text{exact})$ is given by

$$E(\text{exact}) = E(\text{HF}) + E(\text{corr}) \tag{1}$$

where $E(\text{HF})$ and $E(\text{corr})$ represent the Hartree-Fock and correlational contributions, respectively. The HF single-determinant wave function (Ψ_{HF}) of the n electron system in the ground state is expressed by

$$\Psi_{HF} = (n!)^{-1/2} |\chi_1 \chi_2 \cdots \chi_i \chi_j \cdots \chi_n|. \tag{2}$$

The excited-state wave function is written as a linear combination of all possible singly excited determinants, which leads us to the CIS method:

$$\Psi_{CIS} = a_0 \Psi_0 + \sum_{i}^{occ} \sum_{a}^{vir} a_i^a \Psi_i^a . \tag{3}$$

The prediction of oscillator strength f for the excitation requires the calculation of the transition matrix element ($\langle \Psi_{gs} | \hat{d} | \Psi_{es} \rangle$):

$$f = \frac{8 m \pi^2 \nu}{3he^2} \langle \Psi_{gs} | \hat{d} | \Psi_{es} \rangle^2, \tag{4}$$

where Ψ_{gs} and Ψ_{es} represent the wave function of ground state and excited state, respectively, and $\hat{d}$ is dipole moment operator.

In general, the CIS wave function does not present an improvement over the HF wave function, since this approach also neglects correlation effects due to double and higher excitations.

The CIS calculation can be improved by the inclusion of some effects of electronic correlation via second-order Møller-Plesset perturbation theory,

$$\Delta E_{CIS-MP2} = -\frac{1}{4} \sum_{i<j}^{occ} \sum_{a<b}^{vir} \frac{\langle \Psi_{CIS} | H | \Psi_{ij}^{ab} \rangle^2}{\epsilon_a + \epsilon_b - \epsilon_i - \epsilon_j - \Delta_{CIS}}$$

$$- \frac{1}{36} \sum_{i<j<k}^{occ} \sum_{a<b<c}^{vir} \frac{\langle \Psi_{CIS} | H | \Psi_{ijk}^{abc} \rangle^2}{\epsilon_a + \epsilon_b + \epsilon_c - \epsilon_i - \epsilon_j - \epsilon_k - \Delta_{CIS}}, \tag{5}$$

where Δ_{CIS} is the difference between the CIS excitation and ground-state energies. The $\Delta E_{CIS\text{-}MP2}$ can be added to E_{CIS} to define $E_{CIS\text{-}MP2}$ for an excited state. The corresponding eigenvalues are the orbital energies $\epsilon_1, \ldots, \epsilon_n$ involving the labels $i,j,k, \ldots$ for occupied spin orbitals and labels $a,b,c, \ldots$ for virtual spin orbitals.

The inclusion of only doubly excited configurations leads to the CID method,

$$\Psi_{CID} = a_0 \Psi_0 + \sum_{i<j}^{occ} \sum_{a<b}^{vir} a_{ij}^{ab} \Psi_{ij}^{ab} . \tag{6}$$

When both single and double virtual excitations are included, the CISD wave function is obtained as

$$\Psi_{CISD} = a_0 \Psi_0 + \sum_{i}^{occ} \sum_{a}^{vir} a_i^a \Psi_i^a + \sum_{i<j}^{occ} \sum_{a<b}^{vir} a_{ij}^{ab} \Psi_{ij}^{ab} . \tag{7}$$

An approximation of the effects of triple substitution is available through the QCISD T), where three-particle excitations are included by means of the fourth-order Møller-Plesset (MP4) perturbation theory.[14,15]

The contribution of triple substitutions ($ijk \rightarrow abc$) to the fourth-order correlation energy is evaluated as

$$E_T^{(4)} = -\frac{1}{36} \sum_{ijk}^{occ} \sum_{abc}^{vir} (\epsilon_a + \epsilon_b + \epsilon_c - \epsilon_i - \epsilon_j - \epsilon_k)^{-1} |\Psi_{ijk}^{abc}|^2 . \tag{8}$$

2. Nonlinear optical surface response

The electric polarization P can be expanded in terms of the electric field as

$$P = \chi^{(\omega)} E + \chi^{(2\omega)} E^2 + \chi^{(3\omega)} E^3 + \cdots, \tag{9}$$

where $\chi^{(\omega)}, \chi^{(2\omega)}, \chi^{(3\omega)}, \ldots$ are tensors of the linear polarizability, the first-order and the second-order hyperpolarizabilities, respectively, and so on. In this work, we deal with $\chi^{(2\omega)}$ representing a second-harmonic contribution. Within the electric-dipole approximation, $\chi^{(2\omega)}$ vanishes for bulk NiO due to the inversion symmetry of the crystal, but it is allowed at the surface where inversion symmetry is broken. Thus, in the electric-dipole approximation, SHG is an ideal probe of the surface d-d intragap transitions.

We consider an expression for the second-order polarization

$$P_i = \varepsilon_0 \chi_{ijk}^{(2\omega)} E_j E_k , \tag{10}$$

where

$$\chi^{(2\omega)}_{ijk}(\omega)=\frac{\rho_0}{\varepsilon_0}\sum_{\alpha\beta\gamma}\left[\langle\gamma|d_i|\alpha\rangle\langle\overline{\alpha|d_j|\beta\rangle\langle\beta|d_k|\gamma}\rangle\times\frac{\dfrac{f(E_\gamma)-f(E_\beta)}{E_\gamma-E_\beta-\hbar\omega+i\hbar\delta}-\dfrac{f(E_\beta)-f(E_\alpha)}{E_\beta-E_\alpha-\hbar\omega+i\hbar\delta}}{E_\gamma-E_\alpha-2\hbar\omega+2i\hbar\delta}\right],\quad \{i,j,k\}\in\{x,y,z\} \tag{11}$$

is the second-harmonic susceptibility tensor. It is derived from the second-order perturbation theory for the density matrix and the details are given in Ref. 13. In this formula, f is the Fermi distribution, which is unity for the ground state, and vanishes otherwise. ρ_0 is the unperturbed electronic density and $\langle\alpha|d_{i,j,k}|\beta\rangle$ are the matrix elements of the dipole moment $\boldsymbol{d}=(d_x,d_y,d_z)$. The overline denotes the symmetrization needed to fulfill the symmetry upon interchanging the two incident photons. The transition dipole matrix elements over two Slater determinants are computed according to [see Eq. (2)]

$$\begin{aligned}\langle\alpha|\boldsymbol{d}|\beta\rangle&=\left\langle\frac{1}{\sqrt{n!}}\left|\chi_1^\alpha\chi_2^\alpha\cdots\chi_i^\alpha\cdots\chi_n^\alpha\right|\boldsymbol{d}\right|\frac{1}{\sqrt{n!}}\\&\quad\times|\chi_1^\beta\chi_2^\beta\cdots\chi_i^\beta\cdots\chi_n^\beta|\Big\rangle\\&=\sum_{i,j=1}^{n}(-1)^{i+j}\langle\chi_i^\alpha|\boldsymbol{d}|\chi_j^\beta\rangle\boldsymbol{M}_{ij},\end{aligned} \tag{12}$$

where $\boldsymbol{M}_{ij}$ are the minors of the matrix composed of the overlaps between single-particle wave functions

$$\boldsymbol{M}=\begin{pmatrix}O_{11}^{\alpha\beta}&O_{12}^{\alpha\beta}&\cdots&O_{1n}^{\alpha\beta}\\O_{21}^{\alpha\beta}&O_{22}^{\alpha\beta}&\cdots&O_{2n}^{\alpha\beta}\\\vdots&\vdots&\cdots&\vdots\\O_{n1}^{\alpha\beta}&O_{n2}^{\alpha\beta}&\cdots&O_{nn}^{\alpha\beta}\end{pmatrix}. \tag{13}$$

For the NiO(001) surface, the symmetry analysis gives the only nonvanishing tensor elements resulting from the crystallographic structure of an undistorted cubic lattice:

$$\chi^{(2\omega)}_{ijk}=\left(\begin{array}{ccc|ccc}0&0&0&0&\chi^{(2\omega)}_{xxz}&0\\0&0&0&\chi^{(2\omega)}_{yyz}&0&0\\\chi^{(2\omega)}_{zxx}&\chi^{(2\omega)}_{zyy}&\chi^{(2\omega)}_{zzz}&0&0&0\end{array}\right). \tag{14}$$

To calculate $\chi^{(2\omega)}$ related to surface antiferromagnetism, we need spin-orbit coupling to be included. This however is beyond the scope of this paper and will be the subject of a forthcoming paper.

Based on the SHG tensor we compute nonlinear optical properties of the system. The second-harmonic electrical-field projection on the optical plane of the analyzer is given in the short form notation[16] by

$$\begin{aligned}E(2\omega;\Theta,\Phi,\varphi)=2i\,\delta z\frac{\omega}{c}|E_0^{(\omega)}|^2&\begin{pmatrix}A_pF_c\cos\Phi\\A_s\sin\Phi\\A_pN^2F_s\cos\Phi\end{pmatrix}\\&\times\left(\begin{array}{ccc|ccc}\cdot&\cdot&\cdot&\cdot&\cdot&\cdot\\\cdot&\chi^{(2\omega)}_{ijj}&\cdot&\cdot&\chi^{(2\omega)}_{ijk}&\cdot\\\cdot&\cdot&\cdot&\cdot&j\neq k&\cdot\end{array}\right)\\&\times\begin{pmatrix}f_c^2t_p^2\cos^2\varphi\\t_s^2\sin^2\varphi\\f_s^2t_p^2\cos^2\varphi\\2f_st_pt_s\cos\varphi\sin\varphi\\2f_cf_st_p^2\cos^2\varphi\\2f_ct_pt_s\cos\varphi\sin\varphi\end{pmatrix},\end{aligned} \tag{15}$$

where Θ, Φ, and φ are the angle of incidence, polarization of the incident photon, and polarization of the output photon, respectively. The nonlinear response depends as well on the optical properties of the system. Introducing notations for the frequency-dependent refraction index of the material $n=\sqrt{\varepsilon(\omega)}$ and $N=\sqrt{\varepsilon(2\omega)}$, the other parameters can be expressed as $f_s=\sin\Theta/n$, $f_c=\sqrt{1-f_s^2}$—projections of the wave vector in the system, $t_p=2\cos\Theta/(n\cos\Theta+f_c)$ and $t_s=2\cos\Theta/(\cos\Theta+nf_c)$—linear transmission coefficients, and $A_p=2\pi T_p/\cos\Theta$ and $A_s=2\pi T_s/\cos\Theta$—transmission field amplitudes. δz means the thickness of the system (in our case, equal to lattice constant of 4.1684 Å).

The intensity of the SHG response can then be obtained from

$$I(2\omega;\Theta,\Phi,\varphi)=\varepsilon_0c_0|E(2\omega;\Theta,\Phi,\varphi)|^2. \tag{16}$$

B. Method implementation

The smallest suitable cluster to simulate bulk NiO consists of one Ni^{2+} ion and six nearest-neighbor O^{2-} ions forming a cubic crystallographic arrangement with the O_h group,[17] $(NiO_6)^{10-}$. In contrast, the NiO(001) surface has C_{4v} symmetry (considering fivefold crystal-field state), therefore we use a $(NiO_5)^{8-}$ cluster. The isolated cluster and embedded cluster models for the NiO(001) surface are illustrated in Fig. 1. The length of the nickel-oxygen bond has been fixed at 2.0842 Å according to experimental data.[18] This measured value has been commonly used for theoretical models in the unrelaxed case. In order to be able to treat materials with larger surface relaxation, the geometry of the cluster should be optimized. For the geometry optimization on the QCISD level, one must have a possibility to compute forces on the same level of theory. Schemes that evaluate the gradient of generic CI energies have been available for several years.[19,20] Computation of the forces for the simplest CIS method is described in Ref. 8. Formulas for the analytical evaluation of energy gradients in quadratic configuration-interaction theory, such as QCISD are derived in Ref. 14. All of these methods are implemented in GAUSSIAN98. For the relaxed case, we would therefore not expect very strong ef-

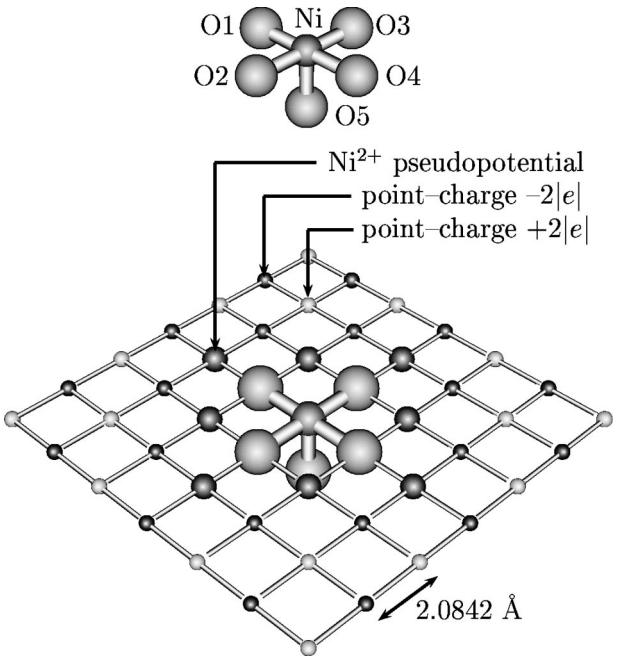

FIG. 1. The $(NiO_5)^{8-}$ cluster and embedded cluster models of the NiO(001) surface (only the surface charges are shown).

fects since the surface of NiO is nonpolar and the most stable geometry is quite close to the truncated bulk one. An experiment[21] showed that surface relaxations are 0–4 % for the first spacing and −4–4 % for the first-layer bucking. This supports our choice of the unrelaxed geometry. In the case of Fe_2O_3 or Al_2O_3, where surface relaxation may play a major role, a prior geometry optimization is necessary.[22–24] In order to correctly account for the electrostatic environment due to the rest of an ionic solid crystal, the simplest possible way is to embed the bare cluster in a set of point charges located at the lattice sites representing the Madelung potential in the framework. The point charges at the edges of the calculated slab are fractional.[25] In the vicinity of the quantum cluster, the point charges were exchanged by effective core potentials (ECP's) with charge +2; for this purpose we used magnesium cores $1s^22s^22p^6$ deprived of two valence electrons in order to simulate Ni^{2+} ions. This allows for the proper description of the Pauli repulsion within the cluster and the nearest-neighboring point charges and prevents a flow of electrons from O^{2-} ions to the positive charges.[26] The structure of the NiO(001) surface was assumed fixed for long-range contributions of the semi-infinite Madelung potential (15×15×7 ions). For the bulk system, our infinite Madelung potential was represented by 15×15 ×15 ions.

For the ground state, we employ a single-point calculation based on the unrestricted HF (UHF) level of theory. As a basis set for the Ni^{2+} ion, we use the valence Los-Alamos basis and double-ζ and effective core potentials (LANL2DZ ECP).[27] The oxygen basis set was a 6-31G* basis.[28] The first step of our excitation calculation is always the CIS calculation in order to estimate excitation spectrum, oscillator strength, and band gap. The basis sets used in these calculations are almost the same as ground-state calculations, except that we add one diffuse function into the oxygen basis set (6-31+G* basis),[29] which is necessary for the excited state calculation.

The next step is to study the electronic correlation effects on the properties of NiO such as d-d transitions. At the correlated level of theory, the correlated increments, namely, CID, CISD, QCISD, and QCISD (T) were compared with CIS. We performed these calculations of five triplet states for d-d transitions:

$$^3B_1[(d_{xz})^2,(d_{yz})^2,(d_{xy})^2,(d_{3z^2-r^2})^1,(d_{x^2-y^2})^1],$$

$$^3E[(d_{xz})^1,(d_{yz})^2,(d_{xy})^2,(d_{3z^2-r^2})^2,(d_{x^2-y^2})^1,$$

and

$$(d_{xz})^2,(d_{yz})^1,(d_{xy})^2,(d_{3z^2-r^2})^2,(d_{x^2-y^2})^1],$$

$$^3B_2[(d_{xz})^2,(d_{yz})^2,(d_{xy})^1,(d_{3z^2-r^2})^1,(d_{x^2-y^2})^2],$$

$$^3A_2[(d_{xz})^2,(d_{yz})^2,(d_{xy})^1,(d_{3z^2-r^2})^2,(d_{x^2-y^2})^1],$$

and

$$^3E[(d_{xz})^1,(d_{yz})^2,(d_{xy})^2,(d_{3z^2-r^2})^1,(d_{x^2-y^2})^2$$

and

$$(d_{xz})^2,(d_{yz})^1,(d_{xy})^2,(d_{3z^2-r^2})^1,(d_{x^2-y^2})^2].$$

These methods allow us to take into account a part of the electronic correlation in both ground and excited states. All *ab initio* embedded calculations were done with the GAUSSIAN98 package.[30]

III. RESULTS AND DISCUSSION

A. Ground state

First, we consider the ground-state electronic structure of an embedded cluster modeled as a 15×15×7 (seven layers deep) point-charge lattice of the NiO(001) surface. The $3d^8$ configuration at the NiO(001) surface has the $^3B_1$ electronic state as its ground state $[(d_{xz})^2,(d_{yz})^2,(d_{xy})^2,(d_{3z^2-r^2})^1,(d_{x^2-y^2})^1]$. In a C_{4v} symmetry, there are four different energy levels, related to the degenerate $d_{xz}(d_{yz})$ orbitals, the d_{xy} orbital, the $d_{3z^2-r^2}$ orbital, and the $d_{x^2-y^2}$ orbital, respectively. More insight in the electronic structure is obtained from the calculated density of states (DOS) of the ground state following Mulliken population analysis, which is shown in Fig. 2. For the description of the DOS, two different sets of orbitals are assigned to the two spins based on an UHF calculation.

Figure 2(a) shows the calculated DOS of the majority spin of the ground state. The lower and upper valence bands predominantly exhibit Ni(3d) and O(2p) characters, respectively. There are altogether 15 electron states between -11.97 and -8.16 eV and 5 states between -17.14 and -15.51 eV which correspond to $2p$ and $3d$ orbitals, respectively, of the O^{2-} and Ni^{2+} ions in the embedded $(NiO_5)^{8-}$ cluster. Some of these states are degenerate. The main character of the localized $3d$ orbitals consists of four electronic states such as $d_{x^2-y^2}$, $d_{3z^2-r^2}$, $d_{xz}(d_{yz})$, and d_{xy}, respectively. The va-

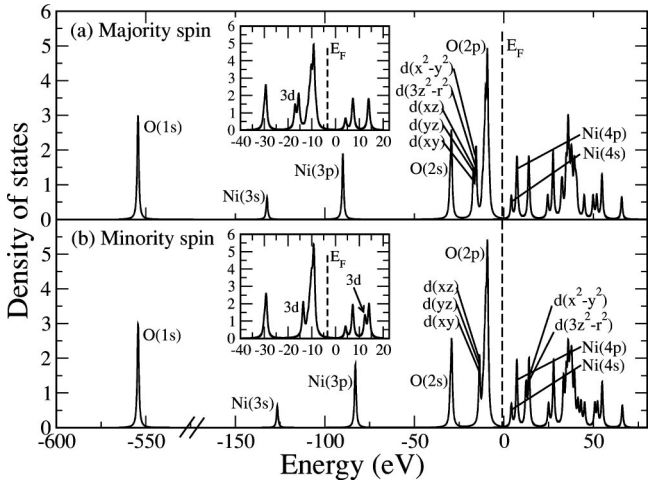

FIG. 2. Density of states broadened by a Lorentzian with the full width at half maximum (FWHM) of 0.5 eV.

lence band has O $(2p)$ states at the upper edge leading to a charge-transfer gap in our study. The four lowest unoccupied orbitals are the $4s$ and $4p$ orbitals of the Ni^{2+} ion.

The DOS of the minority spins is given in Fig. 2(b). The valence band consists of the O $(2p)$ states in the energy range (-11.70, -8.98) eV. The latter comprise the d_{xy} orbital (about -13.69 eV) and the degenerate $d_{xz}(d_{yz})$ orbitals at an energy of -13.66 eV. The lower edge of the conduction bands also consists of the $4s$ and $4p$ orbitals. The vicinity of the unoccupied Ni $(4s,4p)$ orbitals is mainly of Ni-$3d$ character in an e_g level ($d_{3z^2-r^2}$ and $d_{x^2-y^2}$).

The detailed Mulliken procedure for this embedded cluster also shows the net atomic charge and spin values, see Table I. Note, the atomic labels in Table I are given in Fig. 1. According to a Mulliken population analysis, the Ni and O atoms are not fully ionized, and have explicit charges of $+1.1$ and -1.8, respectively. The net atomic spin resulting from our embedded cluster calculation is similar to the data obtained by Towler *et al.*[31] employing a different approach.

B. Charge-transfer transitions and band gap

Although the CI calculation does not directly provide information about the band gap (the band gap corresponds to experiments with variable particle number, such as x-ray photoemission, and must be obtained from a Green-function method such as GW or by identifying the ionization potential and electron affinity that will correspond to the highest occupied molecular orbital and lowest occupied molecular orbital (HOMO-LUMO) gap, we estimate it by keeping a track on transitions between ground and excited states from the CIS calculation possessing the symmetry of the $2p$ oxygen (HOMO state) and $4s$ nickel (LUMO) states, respectively. The lowest excited state, where this transition is strongly expressed, has an energy of 7.6 eV (the corresponding CIS coefficient is $\approx 82\%$). This is much larger than the experimental value [4.0–4.3 eV (Refs. 32 and 33) in bulk NiO] or the result of a GW calculation (5.5 eV) by Aryasetiawan *et al.*[7] Such a large discrepancy has two origins: the importance of the correlation effects is not accounted for properly on the CIS level and the fact that the excitation energy can be identified with the HOMO-LUMO gap only in the case of infinite particle number. Therefore, to improve the gap energy we include some of the electronic correlation beyond the CIS method via second-order Møller-Plesset perturbation theory called CIS-MP2 calculation. We found a smaller gap of 6.8 eV, indicating that correlation energy is of importance here. Even though our band gap between O-$2p$ and Ni-$4s$ state is not in good agreement with experimental data for both Mott-Hubbard and charge-transfer insulators ($d \rightarrow d$ and $p \rightarrow d$ characters, respectively), it provides us with an appropriate description of the low-lying d-d intragap excitations that are of interest for magnetic applications.

C. Excitation spectra of NiO(001) surface

Using a Lorentzian level broadening with 0.5 eV FWHM, we obtain the density of excited states on the NiO(001) surface from the 300 excitation energies [see Fig. 3(a)]. There are several important implications of these findings. First, in CIS calculation, the d-d transitions lie in the range below 3.0 eV and fall within the band gap of 7.6 eV. These transitions support the results of high-resolution electron-energy-loss spectroscopy (EELS) measurements. Noguera *et al.*[34] mentioned that the EELS experiments have revealed a range of weak absorptions within the gap in the range 0.5-3.0 eV, which have been attributed to orbitally forbidden ($\Delta l = 0$) one- and two-electron bulk and (100) surface d-d excitations. Second, excitations above the gap have a charge-transfer character (O-$2p \rightarrow$ Ni-$4s$, O-$2p \rightarrow$ Ni-$4p$,$5p$, and O-$2p \rightarrow$ Ni-$3d$) or consist of intra-atomic (Ni-$3d \rightarrow$ Ni-$4s$ and Ni-$3d \rightarrow$ Ni-$4p$) transitions, while d-d transitions are not found in this region.

TABLE I. Calculated net atomic charges (q) and net atomic spin (δn_s) carried out by Mulliken population analysis. The results of Ref. 31 for true antiferromagnetic type II (AF_2) and hypothetical ferromagnetic (FM) and antiferromagnetic type I (AF_1) configurations of NiO are given for comparison of the spin-density distributions.

This work			Ref. 31		
Atom	q	δn_s	Magnetic configuration	δn_s (Ni)	δn_s (O)
Ni	1.1172	1.8922	NiO (AF_2)	1.923	0.000
O1-O4	-1.8119	0.0208	NiO (AF_1)	1.934	0.024
O5	-1.8697	0.0248	NiO (FM)	1.931	0.069

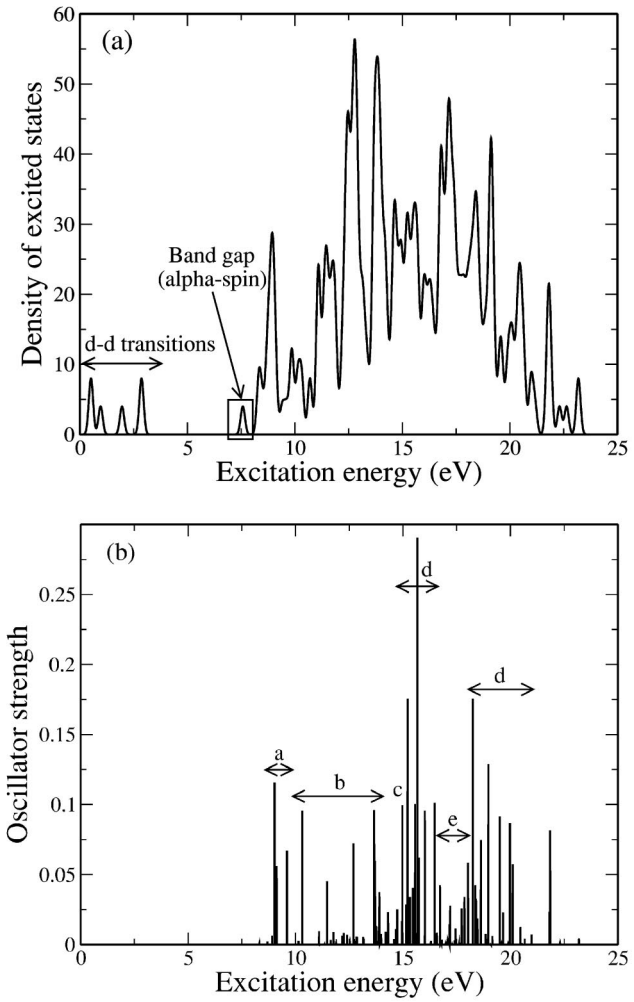

FIG. 3. (a) UV/visible spectra obtained for the NiO(001) surface. (b) Oscillator strengths for the optically allowed transitions. The notations $a,b,c,d,$ and e are used to label each transition such as O $(2p)\rightarrow$Ni $(4s)$, O $(2p)\rightarrow$Ni $(4p)$, O $(2p)\rightarrow$Ni $(3d)$, O $(2p)\rightarrow$Ni $(5p)$, and Ni $(3d)\rightarrow$Ni $(4p)$, respectively.

D. Oscillator strengths and optical absorption spectra

In Fig. 3(b), we plot some of the oscillator strengths of allowed transitions from our 300 vertical excited states in the CIS calculation. It is shown that the oscillator strengths of optically allowed transitions correspond to O $(2p)\rightarrow$Ni $(4s)$, O $(2p)\rightarrow$Ni $(4p)$, O $(2p)\rightarrow$Ni $(3d)$, O $(2p)\rightarrow$Ni $(5p)$, and Ni $(3d)\rightarrow$Ni $(4p)$ transitions labeled as $a-e$ in Fig. 3(b). As an example, consider the group of excitations c for O $(2p)\rightarrow$Ni $(3d)$. It is well known that the experimental band gap results from transitions of type c, which are expected to occur at lower energies in a theory beyond the CIS level due to the correlation effects of the d electrons. In addition, as is clear from Fig. 3(b), the oscillator strengths of these transitions are sufficiently large to make them observable. Hence, the optical absorption spectra (allowed transitions) dominantly arise from the charge-transfer states. However, it should be noted that the d-d transitions and band-gap (in CIS) excitations are forbidden transitions (in linear optics) as the oscillator strength equals to zero.

E. d-d transitions

Our calculation yields the optically active states within the gap of NiO, their character depends on the local symmetry: in the clusters that simulate bulk NiO, the gap states have a charge-transfer character. On the surface, however, a strong contribution of the optically active d-d transitions can be observed. These excited states have energies lower than the charge-transfer excitation, which is important in describing the optical properties of the TMO. An understanding of these transitions is very important for the development of the theory of surface SHG in NiO(001).[35,36]

In Table II, we compare the d-d excitation energies of Ni^{2+} ions on the NiO(001) surface in our highest-level calculation with available theoretical and experimental data. The d-d transitions for bulk NiO are also shown for comparison of surface d-d transitions. These transitions are only related to triplet-triplet excitations. The last column in Table

TABLE II. Calculated d-d excitation energies (eV) of the NiO(001) surface and bulk NiO compared to available experimental and theoretical data from Ref 34.

State	Transition	Excitation energy (eV)		This work	
		Theory (Ref. 34)	Experiment (Ref. 34)	QCISD (T)	Transition
Ni^{2+} surface	$^3B_1\rightarrow{}^3E$	0.65, 0.62, 0.50	0.57, 0.60	0.53	$d_{xz}\rightarrow d_{3z^2-r^2}$
					$d_{yz}\rightarrow d_{3z^2-r^2}$
	$^3B_1\rightarrow{}^3B_2$	1.00, 0.98, 0.83	1.00	1.17	$d_{xy}\rightarrow d_{x^2-y^2}$
	$^3B_1\rightarrow{}^3A_2$	1.30, 1.21	1.30	1.21	$d_{xy}\rightarrow d_{3z^2-r^2}$
	$^3B_1\rightarrow{}^3E$	1.44, 1.38, 1.85	1.62	1.84	$d_{xz}\rightarrow d_{x^2-y^2}$
					$d_{yz}\rightarrow d_{x^2-y^2}$
Ni^{2+} bulk	$^3A_{2g}\rightarrow{}^3T_{2g}$	1.00, 0.81, 0.86	1.13, 1.08	1.13	$d_{xz}\rightarrow d_{x^2-y^2}$
			1.05,1.10		$d_{xy}\rightarrow d_{x^2-y^2}$
					$d_{yz}\rightarrow d_{3z^2-r^2}$
	$^3A_{2g}\rightarrow{}^3T_{1g}$	1.72, 1.81	1.95, 1.86	2.10	$d_{yz}\rightarrow d_{x^2-y^2}$
		2.07, 2.21	1.79,1.87		$d_{xz}\rightarrow d_{3z^2-r^2}$
					$d_{xy}\rightarrow d_{3z^2-r^2}$

TABLE III. Calculated *d-d* excitation energies (eV) of the NiO(001) surface and bulk NiO at differential levels of *ab initio* correlated theory (this work).

State	Transition	Excitation energy (eV)				
		CIS	CID	CISD	QCISD	QCISD (*T*)
Ni^{2+}	$^3B_1 \rightarrow {}^3E$	0.51	0.51	0.52	0.53	0.53
Surface	$^3B_1 \rightarrow {}^3B_2$	0.96	1.02	1.04	1.16	1.17
	$^3B_1 \rightarrow {}^3A_2$	1.96	1.64	1.64	1.32	1.21
	$^3B_1 \rightarrow {}^3E$	2.86	2.61	2.63	2.23	1.84
Ni^{2+}	$^3A_{2g} \rightarrow {}^3T_{2g}$	0.90	0.99	1.01	1.11	1.13
Bulk	$^3A_{2g} \rightarrow {}^3T_{1g}$	2.74	2.53	2.55	2.27	2.10

II shows our predicted transitions at energies of 0.53, 1.17, 1.21, and 1.84 eV. The excited states at the lowest energy are twofold degenerate $d_{xz}(d_{yz}) \rightarrow d_{3z^2-r^2}$ transitions; the one-electron $d_{xy} \rightarrow d_{x^2-y^2}$ transition is at higher energy of 1.17 eV. Additionally, the one-electron $d_{xy} \rightarrow d_{3z^2-r^2}$ transition has a relative energy of 1.21 eV and the energetically highest state is the twofold degenerate $d_{xz}(d_{yz}) \rightarrow d_{x^2-y^2}$ transition at 1.84 eV. In bulk NiO, there are two threefold degenerate excitations ($^3T_{2g}$ and $^3T_{1g}$ excited states). The $^3T_{2g}$ state has triple excitations such as $d_{xz} \rightarrow d_{x^2-y^2}$, $d_{xy} \rightarrow d_{x^2-y^2}$, and $d_{yz} \rightarrow d_{3z^2-r^2}$, while the $^3T_{1g}$ state has $d_{yz} \rightarrow d_{x^2-y^2}$, $d_{xz} \rightarrow d_{3z^2-r^2}$, and $d_{xy} \rightarrow d_{3z^2-r^2}$. The excitation energies, the $^3T_{2g}$ and $^3T_{1g}$ states are about 1.13 and 2.10 eV, respectively. Our calculated excitation energies for *d-d* transitions are in good agreement with the experimental observations and with the theoretical calculations in both surface and bulk NiO.

F. Electronic correlation effects on *d-d* transitions

The partly filled $3d$ shell in solid transition-metal compounds is quite localized on the transition-metal ion and gives rise to large electron correlation effects.[34] Thus, it is necessary to include electronic correlation effects for an accurate description of *d-d* excitations in NiO.[34,37,38]

Our *d-d* transitions for different levels of correlation, such as CID, CISD, QCISD, and QCISD (T), are compared with those obtained from CIS calculation in both surface and bulk NiO (see Table III). When the electronic correlation is enhanced from CID to CISD, QCISD and QCISD (T), the electron correlations significantly decrease the magnitude of excitation energies, as seen in Table III. It has been clearly demonstrated that electronic correlation strongly effects the *d-d* transitions. Only at our highest-level theoretical method such as QCISD (T), the *d-d* transition energies are found to compare well with the experimental data, as shown in Table II. Our bulk *d-d* transitions (1.13 and 2.1 eV) are somewhat higher than the SHG lines by Fiebig *et al.*[3] (1.0 eV and 1.75 eV for $^3A_{2g} \rightarrow {}^3T_{2g}$ and $^3A_{2g} \rightarrow {}^3T_{1g}$, respectively). In the following part, we will calculate and discuss the SHG spectra.

G. SHG intensity

We compute the frequency dependence of the nonlinear susceptibility tensor $\chi_{ijk}^{(2\omega)}(\omega)$ based on two different levels of the treatment of correlations: CID and QCISD with a triple correction. As can be seen from Eq. (11), the notion of wave functions as well as the energies of the states is required. The former give rise to the dipole transition matrix elements, which control the symmetry properties of the spectrum (selection rules) as well as the magnitude of the peaks. The knowledge of the energies is necessary to get the correct position of the peaks. In order to avoid divergences of the expression close to the poles and to ensure the correct symmetry, we applied the broadening of $\delta = 0.27$ eV (i.e., 0.01 hartree) to each of the states. The transition matrix elements $\langle \alpha | d_i | \beta \rangle$ have been computed based on the Slater determinants corresponding to each of the many-body wave functions, Eq. (12), thus neglecting the correction resulting from the virtual transitions [second and third terms in Eq. (7)]. This correction is important to describe the energy of excited states and is taken properly into account, while for the matrix elements it does not play a crucial role. As we do not include spin-orbit coupling, the dipole matrix elements contain two independent contributions from spin-up and spin-down components. Important features of the SHG spectrum (Fig. 4) are the following.

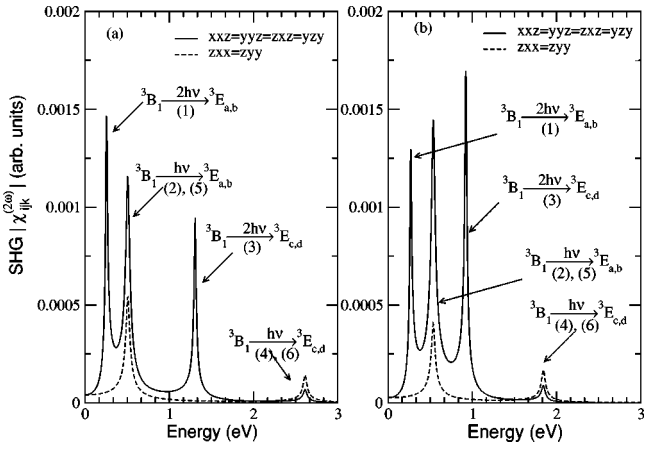

FIG. 4. The nonlinear SHG spectrum of the NiO(001) surface cluster. (a) CID method (b) QCISD (T) method. Note that the $^3E_{a,b}$ and $^3E_{c,d}$ are doubly degenerate excited states corresponding to the energies of 0.51 eV [0.53 eV] and 2.61 eV [1.84 eV] in CID [QCISD (T)], respectively. Corresponding transitions are explained on Fig. 5 together with the energy scheme. The second numbers under the arrows correspond to the dashed curves.

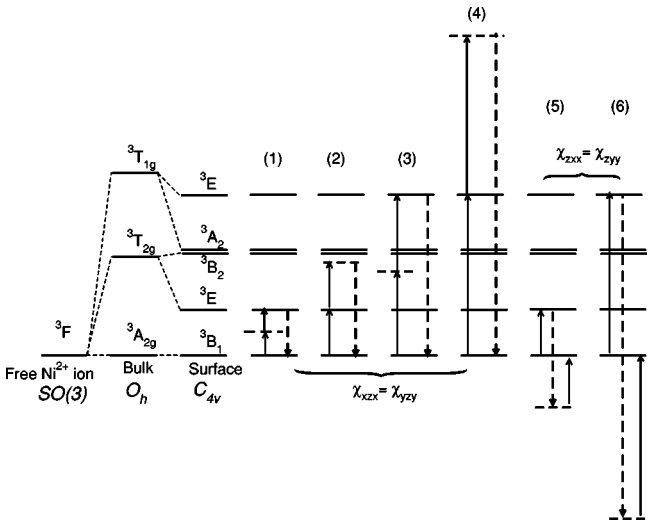

FIG. 5. Energy-level scheme of Ni^{2+} ion in different symmetry environments . The vertical lines denote allowed ED transitions involved in the SHG spectrum (dashed lines correspond to the 2ω transitions). The ^3E states are doubly degenerate and correspond to the $^3E_{a,b}$ and $^3E_{c,d}$ excitations in Fig. 4. The transitions are numbered according to the Fig. 4.

(1) Large difference between the tensor elements: the peaks around 0.35 eV and 0.95 eV are well pronounced only for $|\chi^{(2\omega)}_{xxz}|(=|\chi^{(2\omega)}_{yyz}|=|\chi^{(2\omega)}_{zxz}|=|\chi^{(2\omega)}_{yzy}|)$, while they are absent for $|\chi^{(2\omega)}_{zxx}|=|\chi^{(2\omega)}_{zyy}|$. The tensor element $\chi^{(2\omega)}_{zzz}$, despite it is not forbidden by the selection rules, is accidentally absent in the present theory because of the small number of excited states included in our calculation.

(2) The SHG spectrum originates from all possible combinations of electric-dipole (ED) transitions between the ground state ($^3B_1$) and the two doubly degenerate states of ^3E symmetry (see Fig. 5). Two peaks in the $\chi^{(2\omega)}_{zxx}=\chi^{(2\omega)}_{zyy}$ result from the transitions at fundamental frequency ω from $^3B_1$ to $^3E_{c,d}$ and from $^3E_{a,b}$ to the ground state. The second type of tensor elements has two additional peaks that correspond to $2\hbar\omega$ resonances between these levels.

(3) The nonvanishing tensor elements have nonzero value in the static limit and exhibit Kleinman symmetry[39] with respect to the permutation of the 2ω and ω photons:

$$|\chi^{(2\omega)}_{ijk}|=|\chi^{(2\omega)}_{jik}|=|\chi^{(2\omega)}_{kji}| \quad \text{for} \quad \omega\rightarrow 0. \tag{17}$$

(4) Comparing SHG spectra from CID and QCISD (T) methods, a shift towards lower energies resulting from the higher-level treatment of the correlation can be observed.

Using the nonlinear susceptibility tensor, we compute the intensity of the second-harmonic field (Figs. 6 and 7) according to Eq. (16) for different combinations of the polarization of the incident light at the fundamental frequency (for s polarization, $\varphi=\pi/2$ and for p polarization, $\varphi=0$) and outgoing second-harmonic light (for S polarization, $\Phi=\pi/2$ and for P polarization, $\Phi=0$). The input electric field is taken to be 10^8 V/m, angle of incidence is $\pi/4$, and the complex refractive indices at the frequencies of the fundamental incident and outgoing second harmonic are $n(\omega)$ and $N(2\omega)$,

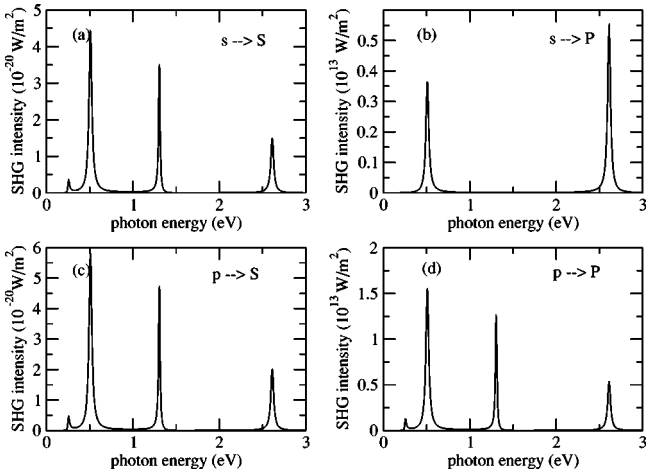

FIG. 6. The nonlinear optical response of NiO(001) surface, based on the CID treatment of the embedded $(NiO_5)^{8-}$ cluster as a function of the incident photon energies for the four possible combinations of the input field and detector.

respectively. Although available from the first-principles calculation on the different levels of theory,[40] $n(\omega)$ and $N(2\omega)$ are taken from experiment[41] in order to make the results more reliable and to avoid artifacts from linear optics. According to the symmetry analysis, the second-harmonic signals in S polarization vanish, and our calculations confirm that, numerically showing the difference in the magnitude between S and P polarizations to be 33 orders of magnitude (Figs. 6 and 7).

It is well known that the SHG response is forbidden for crystals with inversion symmetry within the ED processes. However, taking into account a combination of the magnetic-dipole (MD) and ED processes, one can indeed obtain a second-harmonic response from centrosymmetric NiO in the energy range $2\hbar\omega=1.6$–2.3 eV.[3] The absence of the SHG signal above the Néel temperature and selection rules that define the polarization of the observed signal prove that there

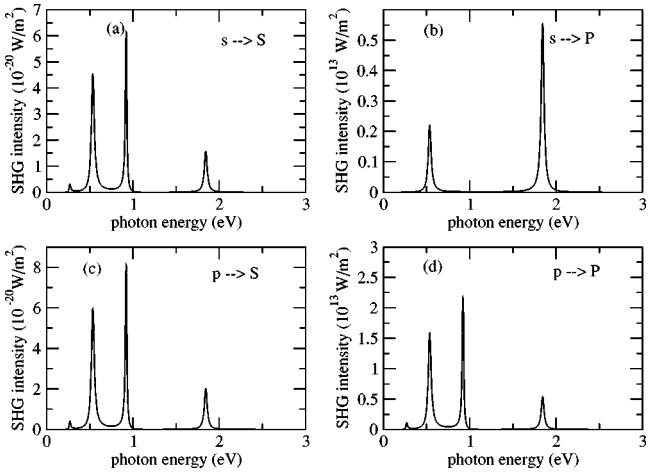

FIG. 7. The nonlinear optical response of NiO(001) surface, based on the QCISD (T) treatment of the embedded $(NiO_5)^{8-}$ cluster as a function of the incident-photon energies for the four possible combinations of the input field and detector.

is no surface contribution in the experiment. In the ED calculation, no SHG intensity is found from the $(NiO_6)^{10-}$ cluster in the cubic lattice.

Our calculation shows the possibility to obtain second-harmonic response from the surface cluster in the range of energies $2\hbar\omega = 1.06–3.68$ eV. This response lies in the region of energies, where the bulk SHG signal has been detected. Thus, under certain conditions, the SHG signal from the surface, which is expected to be considerably weaker, as well as from the bulk, can be observed in one experiment. In the recent investigation by Fiebig *et al.* (Ref. 3), 3 ns light pulses with a pulse energy of about 1 mJ were applied to detect SHG response from the bulk. Although the MD transitions were involved, the intensity is comparable to that observed in noncentrosymmetric compounds such as Cr_2O_3 or $YMnO_3$, where it is exclusively due to ED transitions. Therefore, a larger peak intensity of fundamental light is required to detect SHG response from the surface on the background of the bulk signal. Shorter laser pulses may enable the detection of both surface and bulk contributions in one experiment.

In conclusion, we computed optical properties below the gap of the NiO (001) surface using a series of the configuration interaction methods applied to an embedded cluster model. Our main results are the energies of *d-d* transitions ($^3B_1 \rightarrow {}^3E$, $^3B_1 \rightarrow {}^3B_2$, $^3B_1 \rightarrow {}^3A_2$, $^3B_1 \rightarrow {}^3E$). The importance of effects such as electron correlations is necessary to be taken into account via the QCISD (T) approach. These energies are found to be in good agreement with the available experimental and theoretical data. Using them and the corresponding many-body wave functions, we have calculated the nonlinear optical susceptibilities. This allows us to obtain the intensity of SHG, which has been demonstrated to be a particularly versatile probe of magnetic interfaces and is expected to reveal information on antiferromagnets.

ACKNOWLEDGMENTS

This work has been supported by SFB 418, Forschergruppe 404, and RTN network ''EXCITING.'' The authors would like to thank Dr. M. Nyvlt for his useful discussions.

[1] J. de Boeck and G. Borghs, Phys. World **12**, 27 (1999).
[2] M. Fiebig, D. Fröhlich, B.B. Krichevtsov, and R.V. Pisarev, Phys. Rev. Lett. **73**, 2127 (1994).
[3] M. Fiebig, D. Fröhlich, T. Lottermoser, V.V. Pavlov, R.V. Pisarev, and H.-J. Weber, Phys. Rev. Lett. **87**, 137202 (2001).
[4] A. Dähn, W. Hübner, and K.H. Bennemann, Phys. Rev. Lett. **77**, 3929 (1996).
[5] S. Hüfner and G.K. Wertheim, Phys. Rev. B **8**, 4857 (1973).
[6] A.I. Lichtenstein and M.I. Katsnelson, Phys. Rev. B **57**, 6884 (1998).
[7] F. Aryasetiawan and O. Gunnarsson, Phys. Rev. Lett. **74**, 3221 (1995).
[8] J.B. Foresman, M. Head-Gordon, J.A. Pople, and M.J. Frisch, J. Phys. Chem. **96**, 135 (1992).
[9] J.A. Pople, R. Seeger, and R. Krishnan, Int. J. Quantum Chem., Quantum Chem. Symp. **11**, 149 (1977).
[10] J.A. Pople, M. Head-Gordon, and K. Raghavachari, J. Chem. Phys. **87**, 5968 (1987).
[11] A.I. Boldyrev and J. Simons, J. Phys. Chem. **100**, 8023 (1996).
[12] G.E. Scuseria and H.F. Schaefer, III, J. Chem. Phys. **90**, 3700 (1989).
[13] W. Hübner and K.-H. Bennemann, Phys. Rev. B **40**, 5973 (1989).
[14] J. Gauss and D. Cremer, Chem. Phys. Lett. **150**, 280 (1988).
[15] R. Krishnan, M.J. Frisch, and J.A. Pople, J. Chem. Phys. **72**, 4244 (1980).
[16] J. P. Dewitz, Ph.D. thesis, Martin-Luther-Universität Halle-Wittenberg, Halle, 1999.
[17] G.J.M. Janssen and W.C. Nieuwpoort, Phys. Rev. B **38**, 3449 (1988).
[18] R.W.G. Wyckoff, *Crystal Structures* (Interscience, New York, 1964).
[19] B.R. Brooks, W.D. Laidig, P. Saxe, J.D. Goddard, Y. Yamaguchi, and H.F. Schaefer, III, J. Chem. Phys. **72**, 4652 (1980).
[20] R. Krishnan, H.B. Schlegel, and J.A. Pople, J. Chem. Phys. **72**, 4654 (1980).
[21] M.R.W. Cook and M. Prutton, J. Phys. C **13**, 3993 (1980).
[22] W.C. Mackrodt, R.J. Davey, S.N. Black, and R. Cocherty, J. Cryst. Growth **80**, 441 (1987).
[23] P. Hartman, J. Cryst. Growth **96**, 667 (1989).
[24] J.M. Wittbrodt, W.L. Hase, and H.B. Schlegel, J. Phys. Chem. B **102**, 6539 (1998).
[25] M. Geleijns, C. de Graaf, R. Broer, and W.C. Nieuwpoort, Surf. Sci. **421**, 106 (1999).
[26] T. Klüner, H.-J. Freund, J. Freitag, and V. Staemmler, J. Chem. Phys. **104**, 10 030 (1996).
[27] P.J. Hay and W.R. Wadt, J. Chem. Phys. **82**, 270 (1985).
[28] G.A. Petersson, A. Bennett, T.G. Tensfeldt, M.A. Al-Laham, W.A. Shirley, and J. Mantzaris, J. Chem. Phys. **89**, 2193 (1988).
[29] M.J. Frisch, J.A. Pople, and J.S. Binkley, J. Chem. Phys. **80**, 3265 (1984).
[30] M.J. Frisch *et al.*, computer code GAUSSIAN98 (Revision A.1) (Gaussian Inc., Pittsburgh, PA, 1998).
[31] M.D. Towler, N.L. Allan, N.M. Harrison, V.R. Saunders, W.C. Mackrodt, and E. Aprà, Phys. Rev. B **50**, 5041 (1994).
[32] G.A. Sawatzky and J.W. Allen, Phys. Rev. Lett. **53**, 2339 (1984).
[33] S. Hüfner, J. Osterwalder, T. Riesterer, and F. Hulliger, Solid State Commun. **52**, 793 (1984).
[34] W.C. Mackrodt and C. Noguera, Surf. Sci. **457**, L386 (2000).
[35] M. Trzeciecki and W. Hübner, Phys. Rev. B **62**, 13 888 (2000).
[36] M. Trzeciecki, O. Ney, G.P. Zhang, and W. Hübner, Adv. Solid State Phys. **41**, 547 (2001).
[37] C. de Graaf, R. Broer, and W.C. Nieuwpoort, Chem. Phys. **208**, 35 (1996).
[38] A. Freitag, V. Staemmler, D. Cappus, C.A. Ventrice, K. Al-Shamery, H. Kuhlenbeck, and H.-J. Freund, Chem. Phys. Lett. **210**, 10 (1993).
[39] D.A. Kleinman, Phys. Rev. **126**, 1977 (1962).
[40] J. Hugel and C. Carabatos, J. Phys. C **16**, 6723 (1983).
[41] R.J. Powell and W.E. Spicer, Phys. Rev. B **2**, 2182 (1970).